Change in ultrasonic parameters with loading / unloading process in cyclic loading of aluminium alloy

X. H. Min [a] and H. Kato [b]

a Graduate School of Science and Engineering, Saitama University, Saitama, Japan

b Department of Mechanical Engineering, Saitama University, Saitama, Japan

Abstract:

A local immersion method of the ultrasonic measurement was applied to real-time measurement of the ultrasonic parameters, in aluminiun alloy (A2024-T3) specimens with curved sides during cyclic loadings in fatigue testing. The propagation time of the ultrasonic wave from the surface to the bottom of the specimen changed with time corresponding to the measured local strain of the specimen, and the discrepancy of the measured and estimated transverse strains was discussed with the acousto-elastic effect. From the Fourier spectrum of the bottom echo, the peak intensity, the peak frequency and the average gradient of the transfer function defined as an ultrasonic nonlinearity parameter in response to ultrasonic wave distortion were obtained. The peak intensity and the average gradient of the transfer function changed sinusoidally in a loading cycle, but no change in the peak frequency. Using the Granato and Lücke string model of dislocation damping, the sinusoidal changes of ultrasonic parameters in a loading cycle were discussed by the interaction between dislocations and point defects, which is activated by the low frequency cyclic stress. The ultrasonic parameters were also obtained at some stages in the fatigue process to give a systematic change in the average gradient of the transfer function.

Keywords: Fatigue, Ultrasonic parameters, Dislocation and point defects, Local immersion method, Real-time measurement

1. Introduction

Cyclic loadings in the fatigue process promote formation of dislocation dipoles in metals as a result of mutual trapping of dislocations moving to and fro in response to cyclic changes of stresses to result in change in the attenuation of the acoustic wave as a function of the number of the loading cycle [1]. Granato and Lücke [2,3] developed the string model and formulated the change in the acoustic attenuation in relation with interaction between dislocations and point deflects. Numerous studies have discussed on the fatigue process of metals following the Granato-Lücke string mode. Gremaud et al. [4,5] developed the coupling technique to study the interaction between dislocations and point deflects under applied cyclic stresses.

In recent years, many monitoring methods were developed to evaluate the microstructural evolution in fatigued metals through the dislocation pinning length and the dislocation density. Ogi and co-workers measured the attenuation coefficient and the sound velocity as a function of the loading cycle in the fatigue process of copper and steel [6,7] with the EMAR method, and also the stress-dependent recovery of point defects in deformed polycrystalline aluminium of 99.99% purity [8]. Kenderian et al. [9] used a computer-controlled narrowband ultrasonic pulser/receive system to monitor the change in dislocations density and loop length by measuring the change in the attenuation coefficient and the sound velocity during fatigue of pearlitic rail steel. Johnson studied the ultrasonic dislocation dynamics in Al-0.2 at.% Zn alloy after elastic loading [10], and dislocation damping after plastic deformation in carbon steel [11] by the ultrasonic resonance measurement .

To obtain highly sensitive and reliable ultrasonic data in the fatigue process, many researchers have been focused on the real-time ultrasonic measurement and have developed the contactless methods to overcome shortcomings of the contacting method associated with extra energy loss. In addition, the shear wave has been widely used because it has been pointed out that the shear wave is more sensitive than the longitudinal wave to dislocations [12,13]. In spite of merits, newly developed methods, such as EMAR method, SH method, have limitations such that the data are obtained on/near the surface of materials, and that the ultrasonic wave is not focused on any positions in the thickness direction of materials. To the contrary, by using the immersion method, the ultrasonic wave with higher transfer efficiency can be propagated through the thickness, and can be focused on arbitrary depth in the

specimen. The conventional immersion method, however, has a demerit that the real-time ultrasonic measurement is difficult on the materials under dynamic loading.

The authors have proposed a local immersion method of the ultrasonic measurement [14] to monitor degradation processes of metallic alloys. In the local immersion method, a water bag was used not to contact a transducer directly but to transfer the ultrasonic wave to the specimen through the water. Moreover, the ultrasonic longitudinal wave is focused on a position of an arbitrary depth in material in terms of the lens effect of the transducer [15]. By using the local immersion method, the ultrasonic wave is measured for specimens or large constructions under dynamic loading. And the experimental setup of the local immersion method is easier to perform and takes lower cost than other techniques. In the present work, changes in the ultrasonic parameters in a loading cycle were examined for specimens suffering different stress amplitudes with a local immersion method.

2. Experimental procedures

2.1 Specimen preparation and fatigue testing

Specimens with curved sides as shown in Fig.1 were fabricated from aluminium alloy (A2024-T3) plates so that the specimen axis was parallel to the rolling direction. The chemical composition is tabulated in Table 1, and the plate was subjected to T3 treatment: plates were subjected to solution treatment, cold working, and natural aging successively. Mechanical properties of the specimen are 328 MPa in yield strength (0.2% offset proof stress), 465 MPa in tensile strength, and 20.6% in elongation to fracture in the rolling direction. Specimens were subjected to the fatigue testing under conditions of a stress ratio of 0.05, a frequency of 0.001Hz and stress amplitudes of 50 MPa, 100 MPa and 150 MPa. The frequency of 0.001 Hz was chosen so that the ultrasonic waves were measured on real-time during one loading cycle in the fatigue testing. An experimental setup for measurements of the ultrasonic wave and the local strain is shown in Fig.2. An ultrasonic transducer was set at the center of the specimen, and a strain gage was mounted at a position 20 mm apart from the center of the specimen to obtain a local strain in the loading direction (the longitudinal strain) during cyclic loading. The strain at the center of the specimen was evaluated from the measured strain, reasonably assuming that a ratio of the strain at each position was in

proportion to an area of the cross section of the specimen.

2.2 Ultrasonic measurement

A local immersion method of ultrasonic measurement using a water bag was presented in the previous work [14]. As shown in Fig.3, the ultrasonic transducer generating a longitudinal wave of 20 MHz in frequency with a focal distance of 25.4 mm in water was encapsulated in a water bag of latex membrance with a thickness of 69 μm and was thrust on a specimen. A distance between the transducer and the specimen (the water path) was controlled to be about 7 mm so that the ultrasonic wave was focused on a back surface of the specimen to obtain a larger echo reflected from bottom of the specimen. Under different stress amplitudes, the ultrasonic wave was measured at an interval of 60 seconds in a cycle (for 1000 seconds) during cyclic loading in the fatigue testing and the ultrasonic parameters were obtained through the FFT analysis of the ultrasonic wave. In the ultrasonic measurement, a sampling time was 0.2 ns, and a number of data was 10020 for each measurement.

2.3 Waveform analysis

Typical ultrasonic waves reflected from the surface and the bottom are shown in Fig.4. Waves reflected from the surface and the bottom were subjected to the FFT analysis to obtain the Fourier spectra. The FFT analysis was performed with data of 2048 for each echo. Compared with the surface echo, the bottom echo contains more information of the microstructure since the bottom echo is travelled through interior of the specimen. From the Fourier spectrum of the bottom echo, the peak intensity and the peak frequency were defined as shown in Fig.5. The transfer function $\Gamma(\omega)$ was defined as an ultrasonic nonlinearity parameter in response to an ultrasonic wave distortion, and is given by

$$\Gamma(\omega) = 20\log_{10}\left(\frac{I(\omega)}{I_0(\omega)}\right) \tag{1}$$

where, $I_0(\omega)$ and $I(\omega)$ are the bottom echo spectra before the fatigue testing and

that in a cyclic loading, respectively. Figure 6 shows a typical transfer function. An average gradient of the transfer function was obtained in a frequency range of 14.5～30.5 MHz containing the frequency of the transducer of 20MHz as shown in the figure. The average gradient of the transfer function is equivalent to the frequency dependence of the attenuation, and is related to the change in the peak frequency of Fourier spectrum as shown in Appendix.

3. Results and discussion

3.1 Change in propagation time of the ultrasonic wave in a loading cycle

The specimen was subjected to cyclic loadings of different stress amplitudes. Figure 7 shows a typical change in the longitudinal strain of the specimen at the center in a loading cycle of the stress amplitude of 50 MPa at an early stage of fatigue testing (about 10th cycle from the start).

During cyclic loadings, the ultrasonic measurement was carried out. It was found that travelling times of the ultrasonic wave to the specimen surface and the bottom changed sinusoidally in a loading cycle. In Fig.8, changes in positions of the surface and the bottom echoes in a loading cycle at an early stage of the fatigue testing are shown for different stress amplitudes. The propagation time of the ultrasonic wave from the surface to the bottom was obtained in a loading cycle as shown in Fig.9. The propagation time changed sinusoidally in a loading cycle with time corresponding to the measured strain of the specimen.

Figure 10 shows measured and estimated transverse strains (strain in the thickness direction of the specimen) in a loading cycle for stress amplitudes of 50 MPa and 150 MPa. The measured transverse strain defined as ε_g was calculated from the longitudinal strain (strain in the axial direction) obtained by using the strain gage assuming a Poisson's ratio of 0.343. The estimated transverse strain defined as ε_t was calculated from the propagation time of the ultrasonic wave from the surface to the bottom of the specimen assuming no change in acoustic velocity. From the figure, the estimated transverse strain (ε_t) is almost three times of the measured transverse strain (ε_g). This discrepancy appeared by some causes, such as changes in acoustic velocity, Poisson's ratio, measurement conditions (thickness of the water bag, the focal

position of the transducer), and so on. It was found from the previous report [14] that these factors do not largely affect the strain value except the acoustic velocity. In the present work, influence of the acousto-elastic effect on the discrepancy of the both strains was discussed. Under elastic deformation regime, when the specimen is pulled in the axial direction to make the normal stress (σ) appear in the longitudinal direction of the specimen, the longitudinal acoustic velocity (V) in the thickness direction is changed as follows

$$\frac{(V - V_0)}{V_0} = K\sigma$$

$$= -K\frac{E}{\upsilon}\varepsilon_g \tag{2}$$

where, V_0 and V are the acoustic velocity before a fatigue testing and during a loading cycle, respectively. K, υ and E are the acousto-elastic constant, Poisson's ratio and Young's modulus, respectively.

The estimated transverse strain (ε_t) is expressed by $(TV_0 - T_0V_0)/T_0V_0$. Where, T_0 and T are the propagation time from the surface to bottom of the specimen before a fatigue testing and during a loading cycle, respectively. The measured transverse strain (ε_g) associated with the thickness change of the specimen is given by

$$\varepsilon_g = \frac{(VT - V_0T_0)}{V_0T_0}$$

$$= \frac{V}{V_0}\varepsilon_t + \frac{(V - V_0)}{V_0} \tag{3}$$

Substitution of Eq.(2) into Eq.(3) gives

$$\varepsilon_g = \left(1 - \frac{KE}{\upsilon}\varepsilon_g\right)\varepsilon_t - \frac{KE}{\upsilon}\varepsilon_g \tag{4}$$

Since $\frac{KE}{\upsilon}\varepsilon_g << 1$, the following equation is obtained.

$$\varepsilon_t \cong \left(1+\frac{KE}{\upsilon}\right)\varepsilon_g \tag{5}$$

The value of $(1+KE/\upsilon)$ was calculated to be 2.7 by using the acousto-elastic constant(K) 7.9×10^{-6} MPa^{-1} of the aluminium alloy (A2024-T3) plates [16]. The value explains qualitatively the discrepancy of the measured and estimated strains under elastic regime as shown in Fig.10 (a) because the maximum stress of 105 MPa in the cycle with the stress amplitude of 50 MPa was far less than the yield strength of 328 MPa. In the present work, the acousto-elastic constant(K) of the aluminium alloy (A2024-T3) plates was estimated to be 8.9×10^{-6} MPa^{-1} by using the strain ratio$(\varepsilon_t/\varepsilon_g)$ of 2.9 calculated from Fig.10 (a). It can be concluded that the discrepancy between the measured and estimated transverse strains was mainly affected by the acousto-elastic effect in terms of the values of estimated and referred acousto-elastic constant. Fig.10 (b) shows changes of strains in a loading cycle for the stress amplitude of 150 MPa under plastic regime, and the strain ratio$(\varepsilon_t/\varepsilon_g)$ of 3.5 was larger than that of 2.9 at the stress amplitude of 50 MPa. It was thought that plastic deformation besides the acousto-elastic effect also contributed to discrepancy of the both strains.

3.2 Changes in the ultrasonic parameters in a loading cycle

During cyclic loadings, echoes reflected from the surface and the bottom of the specimen were obtained as shown in Fig.4. In the figure, the echo reflected from the specimen bottom was larger than that from the surface due to focussing of the ultrasonic wave on the bottom. From these echoes, the peak intensity, the average gradient of the transfer function and the peak frequency in one loading cycle were obtained at an early stage of the fatigue testing for different stress amplitudes as shown in Fig.11. The peak intensity and the average gradient of the transfer function of the bottom echo tended to change sinusoidally with time in a loading cycle as shown in Fig.11 (a) and (b). However, no change of the peak frequency was obtained within the accuracy of the present measurement as shown in Fig.11 (c). Changes of the ultrasonic

parameters are due to change in the material structures and the change in the focal position of the transducer following deformation of the specimen [17].

The focal position of the transducer changes sinusoidally in terms of the sinusoidal change of the position of the surface and the bottom echoes as shown in Fig.8. In the measurement for the stress amplitude of 150 MPa, change in water path around 7 mm due to movement and deflection of the specimen was obtained from 6.947 mm to 7.042 mm. Ultrasonic wave reflected from the bottom was measured under different water paths to analyze the change in the ultrasonic parameters. In the steady state measurement, a position of the transducer was deviated from the nominal position by 0.01 mm interval for each measurement, to simulate the change in focal position of the transducer. Figure 12 shows relative changes in the positions of the surface and the bottom echoes due to transducer movement from 6.950 mm to 7.049 mm around original water path of 7 mm. The peak intensity, the average gradient of the transfer function and the propagation time of the ultrasonic wave were changed with varied water path as shown in Fig.13. Although the focal position of the transducer was changed in a range of that as shown in Fig.8, the ultrasonic parameters changed far smaller than those in Fig.11 (a) and (b), and Fig.9. Therefore, it was found changes in the ultrasonic parameters in a loading cycle were independent of the change in the focal position, and hence influence of the change in the internal microstructure during cyclic loading on the ultrasonic parameters was discussed.

Numerous studies have measured changes in acoustic properties of metallic materials under plastic deformation. It is generally known that plastic deformation increases the acoustic attenuation of crystalline materials due to motion of the dislocations [3,11]. Johnson [10] also discussed the interaction of dislocations and defects in Aluminium alloys under elastic deformation.

In order to understand the deformation behavior of metallic materials, it is necessary to understand dynamics of dislocations. Motions of dislocations are controlled by several different interaction mechanisms [4,18,19,20,21]. Granato et al. developed the pinning mechanism to explain the attenuation evolution during loading, holding and unloading processes [3]. The string model for dislocation damping given by Granato and Lücke's [2] has been adopted to represent the relation between the ultrasonic parameters and the dislocation loop length (L) and dislocation density (Λ).

The relations between the attenuation (α) and velocity as a function of the dislocation density (Λ) and dislocation loop length (L) are given by [22]

$$\alpha = \left(\frac{16GBb^2}{\pi^4 C^2} \right) \Lambda L^4 f^2 \tag{6}$$

$$\frac{V - V_0}{V_0} = -\frac{4Gb^2}{\pi^4 C} \Lambda L^2 \tag{7}$$

Substitution of Eqs.(3) and (5) into Eq.(7) gives the following equation.

$$\frac{T - T_0}{T_0} = \left(1 + \frac{\upsilon}{KE} \right) \frac{4Gb^2}{\pi^4 C} \Lambda L^2 \tag{8}$$

where, G is the shear modulus, B the specific damping constant, b the magnitude of the Burger's vector, and υ the Poisson's ratio. C denotes the line tension of the dislocation and is expressed by $2Gb^2/\pi(1-\upsilon)$.

According to Eqs.(6) and (8), the attenuation and the propagation time of the ultrasonic wave are affected by the dislocation density and dislocation loop length of the effective dislocations, which are mobile and can vibrate following the ultrasonic wave induced stress. Change in the peak intensity has a reciprocal relation with the attenuation. Change in the average gradient of the transfer function is associated with changes in the dislocation density and the dislocation loop length due to a relation between the average gradient of the transfer function and frequency dependence of the attenuation given by (see appendix)

$$\frac{d\Gamma(\omega)}{d\omega} = -\frac{20}{\ln 10} \delta \tag{9}$$

Figure 14 shows a schematic representation of the basic interaction between dislocations and point defects in terms of the string model [2]. When an increased stress is applied, a dislocation bows out from point defects and breaks away to result in increasing the dislocation loop length. In terms of Eqs.(6) and (9), the attenuation increases with increasing dislocation loop length to result in decrease of the peak intensity and average gradient of the transfer function. In terms of Eq.(8), the

propagation time of the ultrasonic wave decreased with increasing dislocation loop length. When the stress is decreased, mobile point defects diffuse to the new dislocation lines and pin them again to result in decrease of the dislocation loop length. Therefore, the peak intensity, the average gradient of the transfer function and the propagation time of the ultrasonic wave increase with decreasing dislocation loop length. In Figs.11 (a) and (b), and Fig. 9, tendencies of changes in the peak intensity, the average gradient of the transfer function and the propagation time of the ultrasonic wave are in good agreement with this discussion. However, for the stress amplitude of 50 MPa in Fig.11 (a), it was found that the tendency of change in the peak intensity is not remarkable due to elastic deformation with smaller stress amplitude and the accuracy of the present measurement. When the cyclic stress is reapplied, the dislocations break away and pin again and the dislocation density and dislocation loop length retrieve their values prior to the recovery with time-dependent, which is based upon the Cotrell-bilby Law [3,16,23].

The interaction between dislocations and point defects is activated by applied cyclic and low-frequency stress [4,5]. Therefore, applied different stress amplitudes give different dislocation densities and dislocation loop lengths in a loading cycle. It is assumed that no irreversible dislocation motion and associated permanent dimensional changes occur under the elastic regime without change in dislocation density [10]. Under the plastic regime, the ultrasonic parameters are response to the changes in dislocation density and the dislocation loop length and partial recovery after deformation [11]. When the stress amplitude is increased as shown in Fig.14, due to longer dislocation loop length and larger dislocation density, the peak intensity, the average gradient of the transfer function and the propagation time of the ultrasonic wave at the stress amplitude of 150 MPa change greater than those at the stress amplitude of 50 MPa as shown in Figs.11 (a) and (b), and Fig.9. From Figs.11 (a) and (b), especially for the average gradient of the transfer function, based on incomplete recovery due to time for the stress amplitude of 50 MPa, and partial recovery due to time and irreversible dislocation motion for the stress amplitude of 150 MPa, it was found that the absolute values of the former half cycle were larger than those of the latter half cycle. An intermediate situation for the stress amplitude of 100 MPa is also shown in these figures.

3.3 Changes in the ultrasonic parameters at each stage of the fatigue process

Cyclic deformation behavior is usually dependent on the dislocation structure and its evolution in materials [24]. At each stage of the fatigue process, the dislocation density and the structure change to result in changes in the ultrasonic parameters. The specimen was subjected to the fatigue testing under conditions of a stress ratio of 0.05, a frequency of 10 Hz and stress amplitude of 150 MPa. The fatigue life was 7.985×10^4 cycles. The frequency of 10 Hz was changed to be 0.001 Hz in a loading cycle when the ultrasonic wave was measured on real time at 1.0×10^3 th, 3.0×10^4th, 5.0×10^4th, 7.0×10^4th cycle for the specimen. Changes in the peak intensity and the average gradient of the transfer function were obtained as shown in Fig.15. From the figure, changes in the peak intensity are different in each cycle of the fatigue process, and more complex compared to the change in the average gradient of the transfer function. It was thought that the peak intensity was more sensitive to the ultrasonic measurement conditions in the fatigue testing, but the average gradient of the transfer function was more sensitive to microstructures, such as dislocation. From Fig.15 (b), the average gradient of the transfer function changed sinusoidally with the same tendency at each stage of the fatigue process, and the average value of the cycle increased but the amplitude decreased with increasing number of the loading cycle. From the figure, it was postulated that dislocations moved to and fro in each cycle through the fatigue life, that is, pinning and repining again in response to cyclic changes of stresses, until the fatigue fracture of specimen takes place. From these measurements, it was suggested that the ultrasonic measurement in a loading cycle could give information of successive changes in the dislocation density and dislocation structure at each stage of the fatigue process.

4. Conclusions

By using the local immersion method of ultrasonic measurement with a water bag, real-time measurement of the ultrasonic wave was carried out in a loading cycle in the fatigue testing of different stress amplitudes,

(1) The local immersion method with a water bag was applied to evaluate the microstructural change in the material under cyclic loading.

(2) In a loading cycle, the propagation time of the ultrasonic wave from the surface to the bottom of the specimen changed with time corresponding to the measured local

strain of the specimen, and the discrepancy of the measured and estimated transverse strains was interpreted by the acousto-elastic effect.

(3) The peak intensity, the average gradient of the transfer function of the bottom wave and the propagation time of the ultrasonic wave tended to sinusoidal change with time, and were interpreted as caused by the interaction between dislocations and point defects using Granato and Lücke string model and were dependent on the applied stress in the fatigue testing.

Acknowledgements

The authors would like to thank the Mitsubishi Foundation for financial support.

Appendix

The transfer function is dependent on the frequency, and the average gradient of the transfer function is changed with increasing peak frequency [25]. However, the average gradient of the transfer function and the shift of the peak frequency are associated with attenuation as follows.

(1) Change in average gradient of the transfer function with attenuation

As shown in Fig.A-1, the Fourier spectrum of the ultrasonic wave is approximated as follows,

$$f_0(\omega) = a + b\cos(c\omega) \tag{A-1}$$

where, a, b and c are the constants and ω is the frequency. When the material is damaged, the ultrasonic wave is scattered more through travelling the material to result in decrease in the Fourier spectrum. Assuming that a frequency dependence of the attenuation is given by $(1-\delta\omega)m$, the Fourier spectrum is given by

$$f(\omega) = f_0(\omega)(1-\delta\omega)m \tag{A-2}$$

where, m and δ are the constants. With respect to definition of the transfer function (dB) as a function of the frequency (MHz), the transfer function is given by

$$\begin{aligned}\Gamma(\omega) &= 20\log_{10}\frac{f(\omega)}{f_0(\omega)} = 20\log_{10}\frac{f_0(\omega)(1-\delta\omega)m}{f_0(\omega)} \\ &= 20\log_{10}(1-\delta\omega)m\end{aligned} \tag{A-3}$$

Assuming the value δ is very small, the equation (A-3) is modified as follows,

$$\begin{aligned}\Gamma(\omega) &\cong \Gamma(0) + \Gamma'(0)\omega \\ &= 20\log_{10} m - \left(\frac{20}{\ln 10}\delta\right)\omega\end{aligned} \tag{A-4}$$

Then, the gradient of the transfer function near the origin is expressed by

$$\frac{d\Gamma(\omega)}{d\omega} = -\frac{20}{\ln 10}\delta \tag{A-5}$$

According to the deductive relation, the average gradient of the transfer function is proportional to the proportional constant δ of the frequency. When the frequency dependence of attenuation is positive $(\delta > 0)$, the average gradient of the transfer function is decreased.

(2) Shift of peak frequency with attenuation

The modified Fourier spectrum is given by

$$f(\omega) = \{a + b\cos(c\omega)\}(1 - \delta\omega)m \tag{A-6}$$

Equation (A-6) is differentiated with respect to ω, then

$$f'(\omega) = -bc\sin(c\omega)(1 - \delta\omega)m - \{a + b\cos(c\omega)\}\delta m \tag{A-7}$$

At the peak frequency ω_p of the Fourier spectrum, the derivative $f'(\omega_p)$ becomes 0, which leads to

$$\sqrt{\{b^2c^2(1 - \delta\omega_p) + b^2d^2\}}\sin(c\omega_p + \theta) = -a\delta \tag{A-8}$$

where, θ is given by

$$\theta = \tan^{-1}\left(\frac{b\delta}{bc(1 + \delta\omega_p)}\right) \tag{A-9}$$

When the value of δ is very small $(\delta \cong 0)$,

$$\sin(c\omega_p + \theta) \cong -\frac{a\delta}{bc} \tag{A-10}$$

Therefore, a relation between the peak frequency and the proportional constant δ of the frequency is given by

$$\omega_p \cong -\frac{1}{c}\left\{\tan^{-1}\left(\frac{\delta}{c}\right) + \sin^{-1}\left(\frac{a\delta}{bc}\right)\right\} \tag{A-11}$$

According to the deducted equation (A-11), the peak frequency is shifted to a lower frequency regime with increasing attenuation when the frequency dependence of the attenuation is positive $(\delta > 0)$.

References

(1) John. H. Cantrell and William T. Yost, International Journal of Fatigue, 23 (2001) S487-S490.

(2) A. Granato, K. Lücke, J. Appl. Phys. 27 (1956) 583.

(3) A. Granato, A. Hikata and K. Lücke, Acta Metall. 6 (1958) 470.

(4) G. Gremaud, M. Bujard and W. Benoit, J. Appl. Phys. 61(5) (1987) 1795

(5) M. Bujard, G. Gremaud and W. Benoit, J. Appl. Phys. 62(8) (1987) 3173.

(6) H. Ogi, M. Hirao, K. Minoura, J. Appl. Phys. 81 (1997) 3677.

(7) H. Ogi, T. Hamaguchi, M. Hirao, J. Alloys Comp. 310 (2000) 436.

(8) H. Ogi, A. Tsujimoto, M. Hirao. H. Ledbetter, Acta. Mater. 47(14) (1999) 3745.

(9) S. Kenderian, Tobias P. Berndt, Robert E. Green, Jr, B. Boro Djordjevic, Mater. Sci. Eng. A00 (2002) 1.

(10) W. Johnson, Mater. Sci. Eng. A309-310 (2001) 69.

(11) W. Johnson, J. Alloys Comp. 310 (2000) 423.

(12) E. G. Henneke, Ⅱ, R. E. Green, Jr, Trans. Metall. Soc. AIME 242 (1968) 1073.

(13) E. G. Henneke, Ⅱ, R. E. Green, Jr, Trans. Metall. Soc. AIME 239 (1967) 231.

(14) X. H. Min, H. Kato, Proc. ATEM' 03, JSME-MMD, Nagoya, Sep. 10-12, 2003.

(15) M. Hayakawa and M. Kuroki, Journal of Japanese Society for Non-Destructive Inspection, 50(12) (2001) 785.

(16) M. J. Fisher and G. Herrmann, Review of Progress in Quantitative NDE, Vol.3B, D. O. Thompson and D. E. Chimenti, eds., New York, Plenum Press, (1984) 1283.

(17) X. H. Min, H. Kato, H. Saito, K. Kagayama, Journal of Japanese Society for Non-Destructive Inspection, (Submitted). (In Japanese)

(18) R. Bullough and R. C. Newman, Rep. Prog. Phys. 33 (1970) 101.

(19) R. Bullough and R. C. Newman, Proc. R. Soc. A266 (1962) 198.

(20) A. D. N. Smith, Phil. Mag. 44 (1953) 453.

(21) A. S. Nowick, Acta Met. 3 (1955) 312.

(22) M. Hirao, H. Ogi, N. Suzuki and T. Ohtani, Acta. Mater. 48 (2000) 517.

(23) A. Cottrell and B. Bibly, Proc. Phys. Soc. A 62 (1949) 49.

(24) B. Gong, Z. Wang and Z. G. Wang, Acta Mater. 47(1) (1999) 317.

(25) H. Kato, N. Itoi and K. Kagayama, Journal of Japanese Society for Non-Destructive Inspection, 50(1) (2001) 34.

Captions of the table and the figures

Table 1 Chemical composition of A2024-T3 in mass%.

Fig.1 Shape and dimensions of specimen for fatigue testing.

Fig.2 Setup for measurement of ultrasonic wave and a local strain under fatigue testing.

Fig.3 Schematic representation of immersion method.

Fig.4 Typical ultrasonic waves reflected from surface and bottom.

Fig.5 Typical Fourier spectra of surface and bottom echoes.

Fig.6 Typical transfer function of Fourier spectrum of bottom echo.

Fig.7 Change in longitudinal strain with time in one cycle for stress amplitude of 50 MPa.

Fig.8 Changes in positions of surface and bottom echoes with time in one cycle for different stresses.

Fig.9 Changes in propagation time of ultrasonic wave from surface to bottom in one cycle for different stresses.

Fig.10 Measured and estimated transverse strains in one cycle for stress amplitudes of 50 MPa and 150 MPa.

Fig.11 Changes in ultrasonic parameters of bottom echo spectrum with time in one cycle for different stresses.

Fig.12 Changes in peak position of surface and bottom echoes from the original water path with the transducer movement.

Fig.13 Changes in ultrasonic parameters of bottom echo spectrum with water path without cyclic loading.

Fig.14 Model of the interaction of dislocations and point defects during the cyclic loading. Solid circles are mobile point defects, crosses are strong pinning points.

Fig.15 Changes in ultrasonic parameters in one cycle at each stage of fatigue testing for stress amplitude of 150 MPa.

Fig.A-1 Model for change in the Fourier spectrum of the ultrasonic wave.

Table 1 Chemical composition of A2024-T3 in mass%

Si	Fe	Cu	Mn	Ng	Cr	Zn	Zr+Ti	Ti	Al
0.06	0.18	4.62	0.56	1.53	0.01	0.19	0.03	0.02	RE

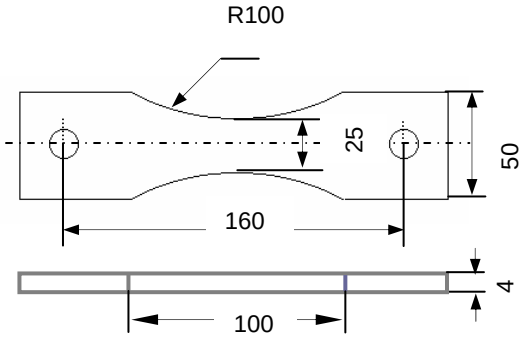

Fig.1 Shape and dimensions of specimen for fatigue testing

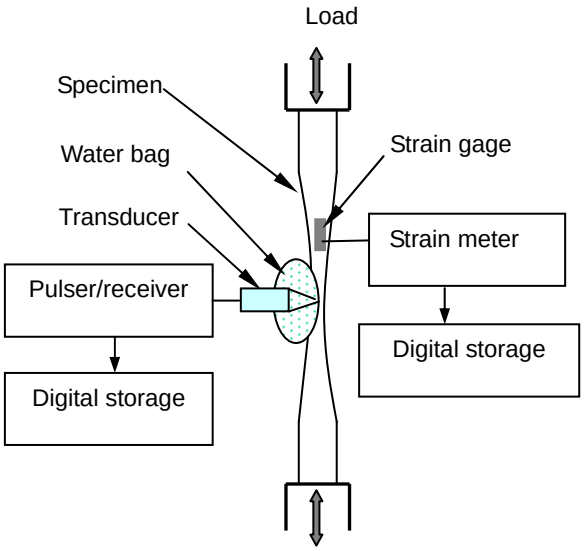

(a) Schematic representation of setup

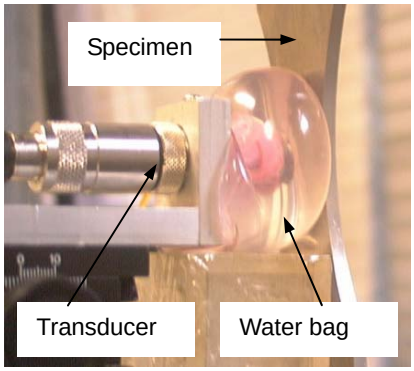

(b) Photograph of setup

Fig.2 Setup for measurement of ultrasonic wave and a local strain under fatigue testing

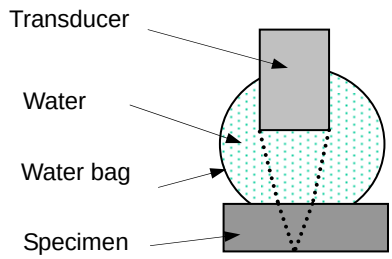

Fig.3 Schematic representation of immersion method

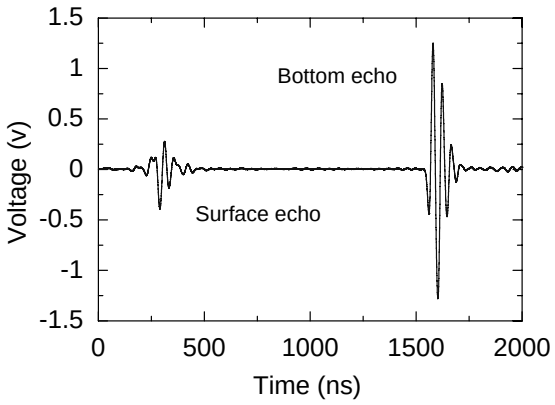

Fig.4 Typical ultrasonic waves reflected from surface and bottom

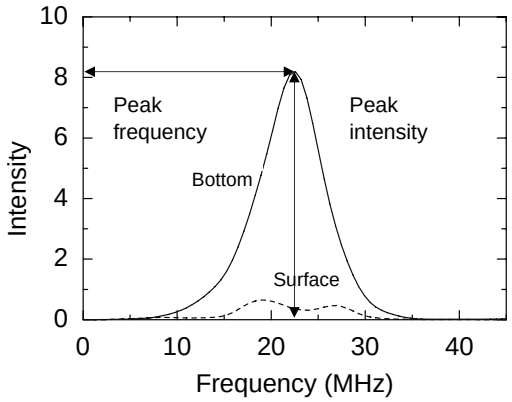

Fig.5 Typical Fourier spectra of surface and bottom echoes

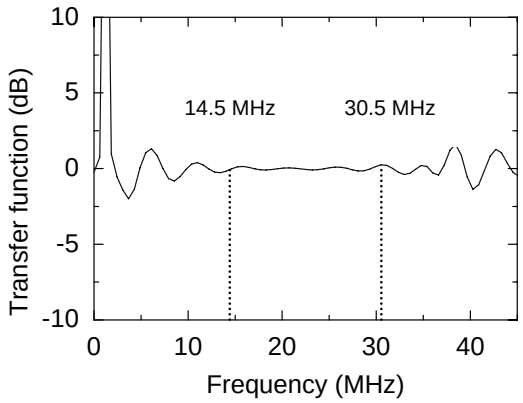

Fig.6 Typical transfer function of Fourier spectrum of bottom echo

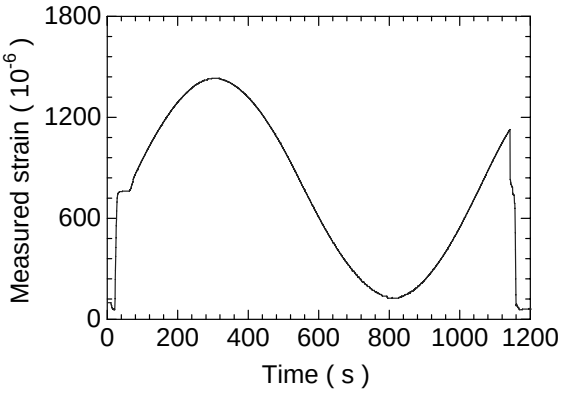

Fig.7 Change in longitudinal strain with time in one cycle for stress amplitude of 50 MPa

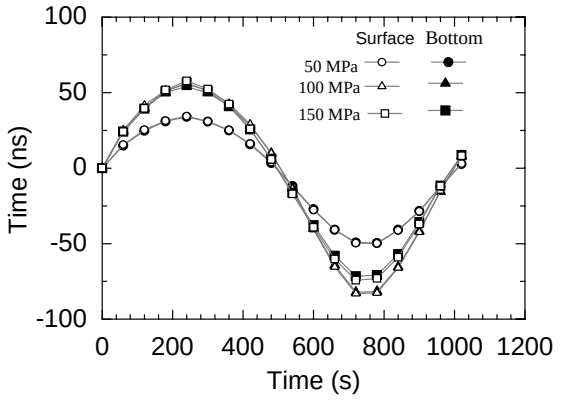

Fig.8 Changes in positions of surface and bottom echoes with time in one cycle for different stresses

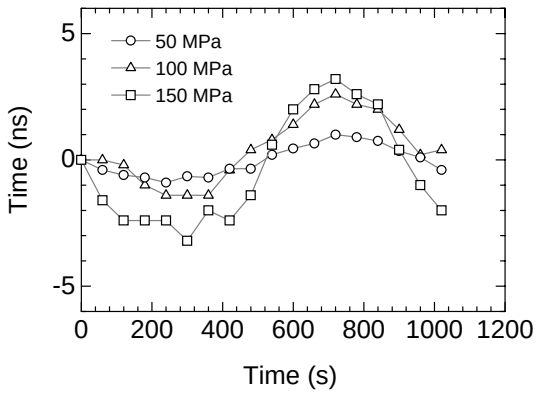

Fig.9 Changes in propagation time of ultrasonic wave from surface to bottom in one cycle for different stresses

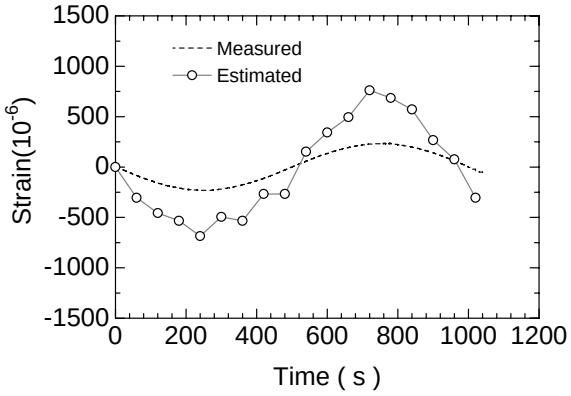

(a) 50 MPa

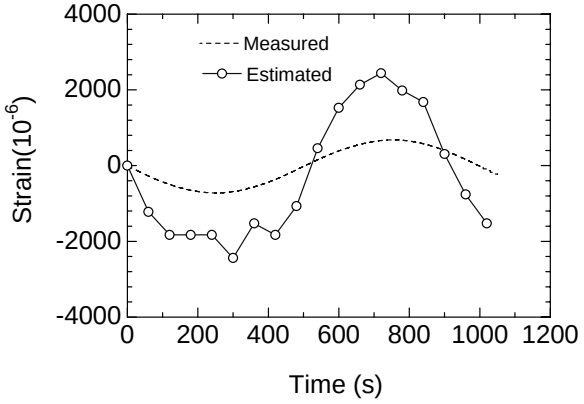

(b) 150 MPa

Fig.10 Measured and estimated transverse strains in one cycle for stress amplitudes of 50 MPa and 150 MPa

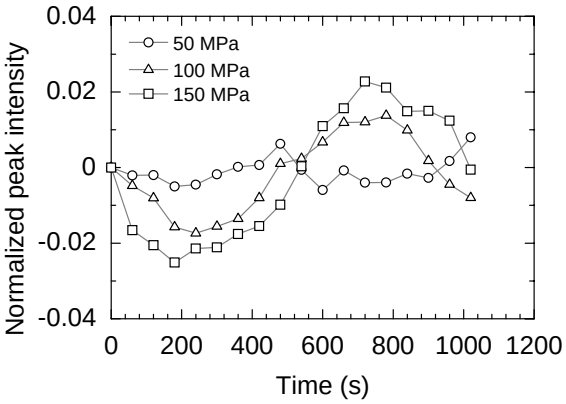

(a) Peak intensity of bottom echo spectrum

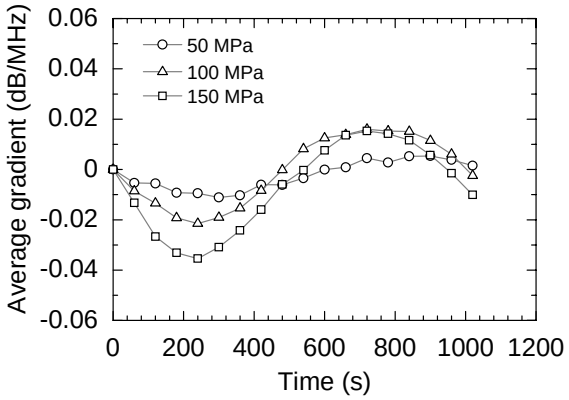

(b) Average gradient of the transfer function

Fig.11 Changes in ultrasonic parameters of bottom echo spectrum with time in one cycle for different stresses

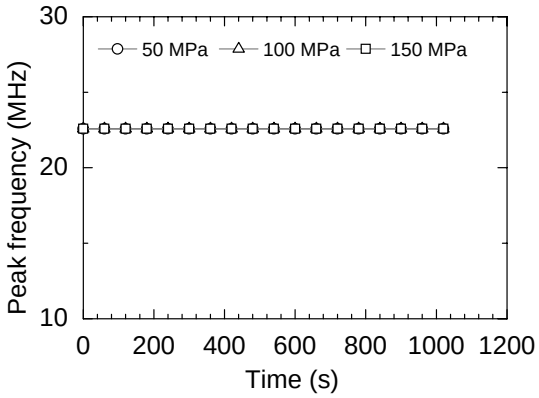

(c) Peak frequency of bottom echo spectrum

Fig.11 (Continued) Changes in ultrasonic parameters of bottom echo spectrum with time in one cycle for different stresses

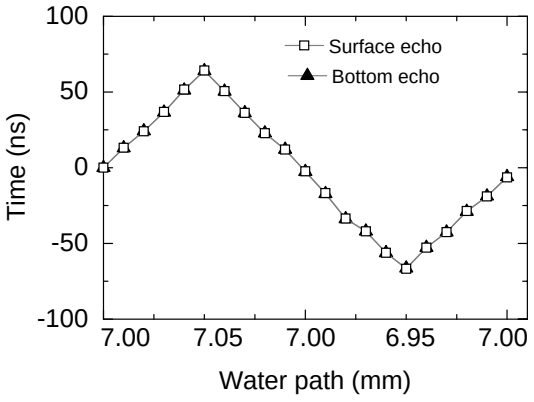

Fig.12 Changes in peak position of surface and bottom echoes from the original water path with the transducer movement

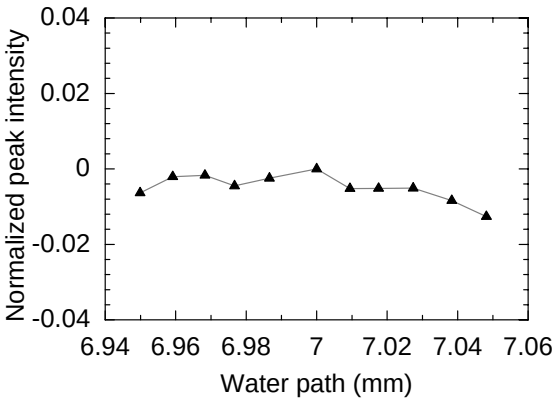

(a) Peak intensity of bottom echo spectrum

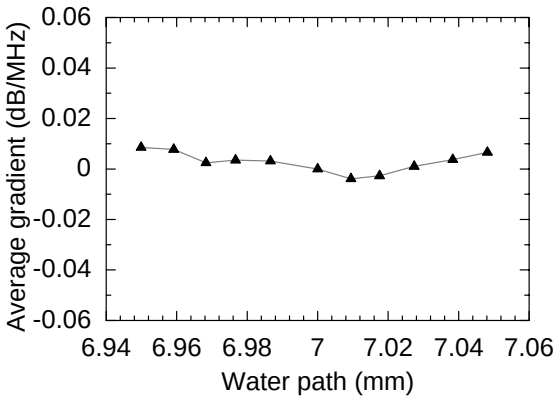

(b) Average gradient of the transfer function

Fig.13 Changes in ultrasonic parameters of bottom echo spectrum with water path without cyclic loading

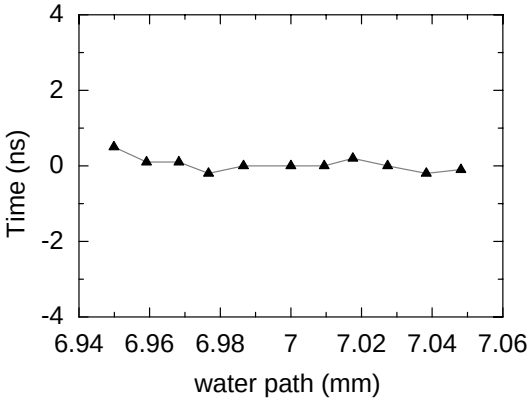

(c) Propagation time of ultrasonic wave

Fig.13 (Continued) Changes in ultrasonic parameters of bottom echo spectrum with water path without cyclic loading

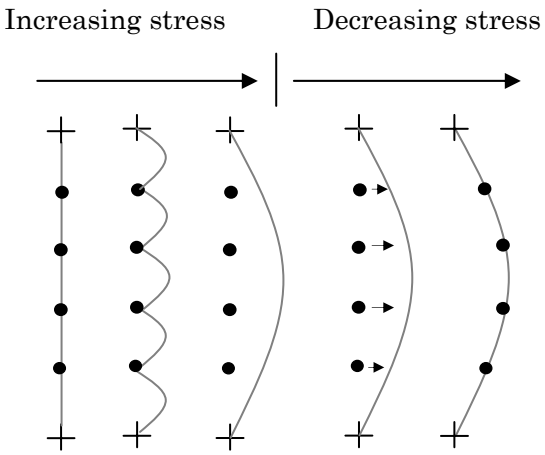

Fig.14 Model of the interaction of dislocations and point defects during the cyclic loading. Solid circles are mobile point defects, crosses are strong pinning points.

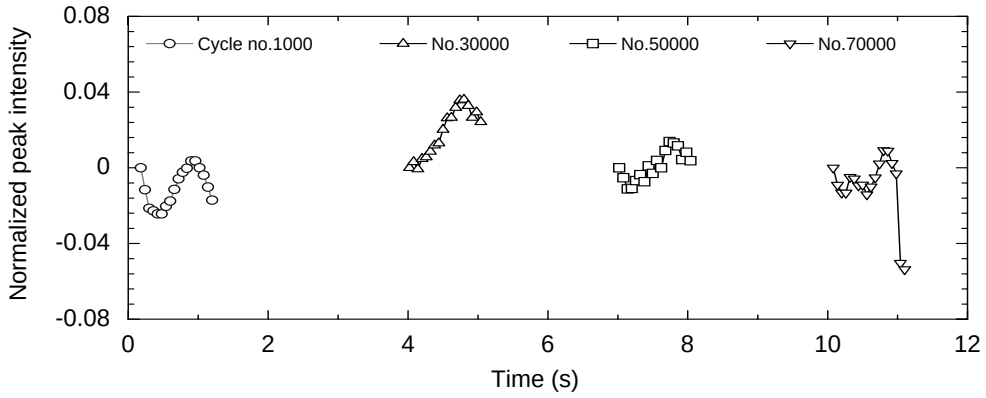

(a) Peak intensity of bottom echo spectrum

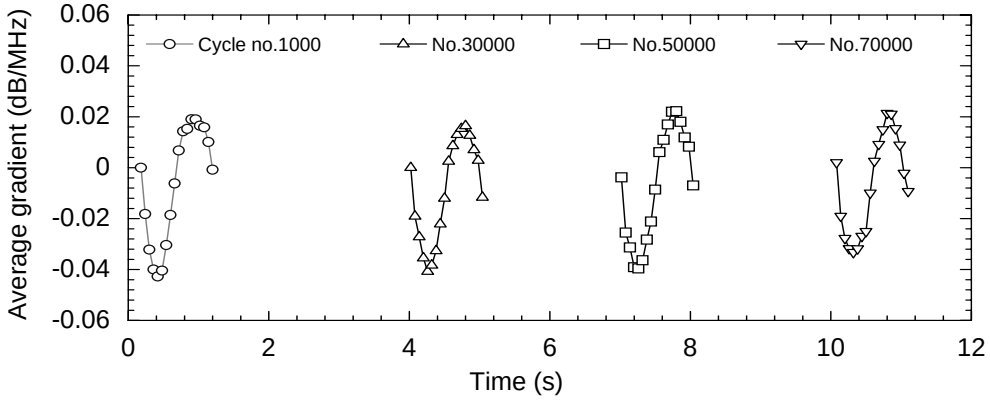

(b) Average gradient of the transfer function

Fig.15 Changes in ultrasonic parameters in one cycle at each stage of fatigue testing for stress amplitude of 150 MPa

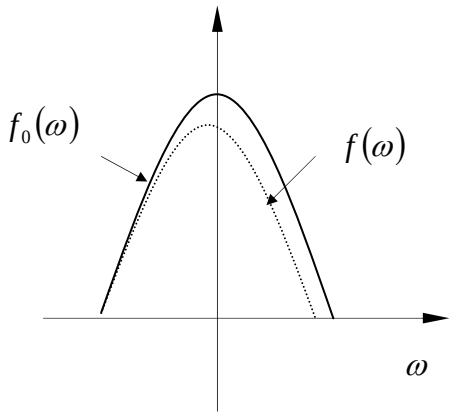

Fig.A-1 Model for change in the Fourier spectrum of the ultrasonic wave

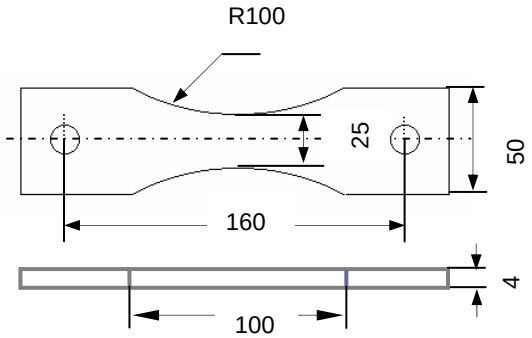

Fig.1 Shape and dimensions of specimen for fatigue testing

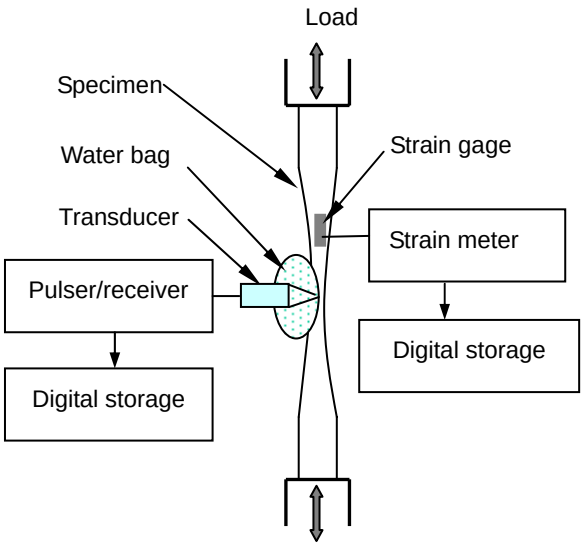

(a) Schematic representation of setup

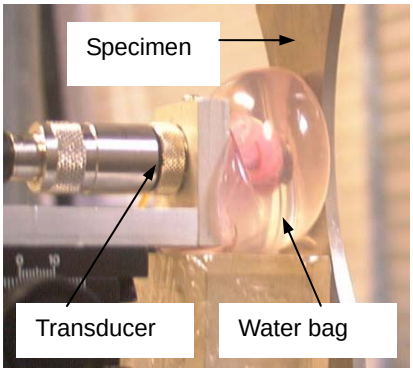

(b) Photograph of setup

Fig.2 Setup for measurement of ultrasonic wave and a local strain under fatigue testing

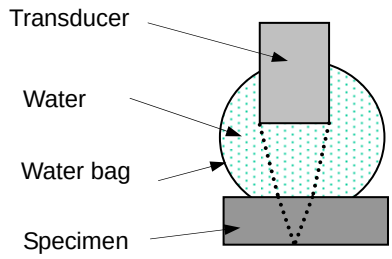

Fig.3 Schematic representation of immersion method

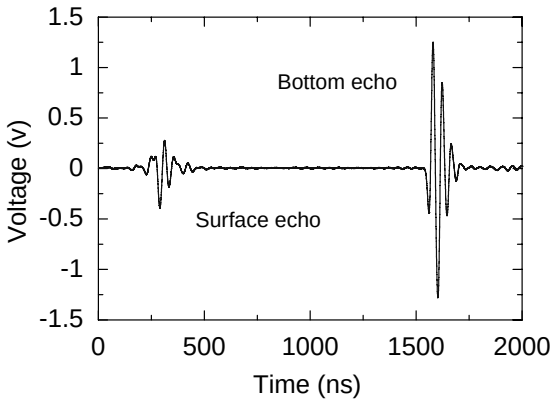

Fig.4 Typical ultrasonic waves reflected from surface and bottom

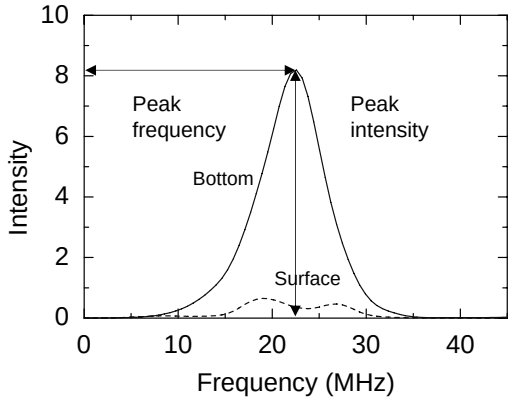

Fig.5 Typical Fourier spectra of surface and bottom echoes

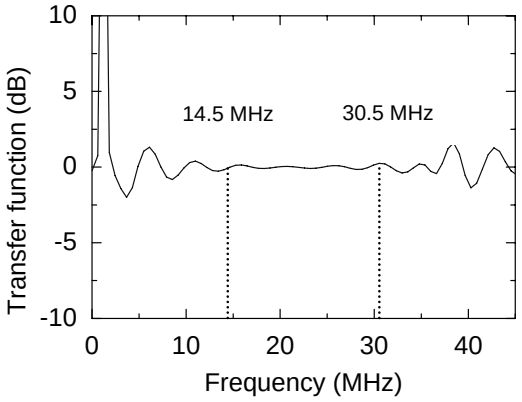

Fig.6 Typical transfer function of Fourier spectrum of bottom echo

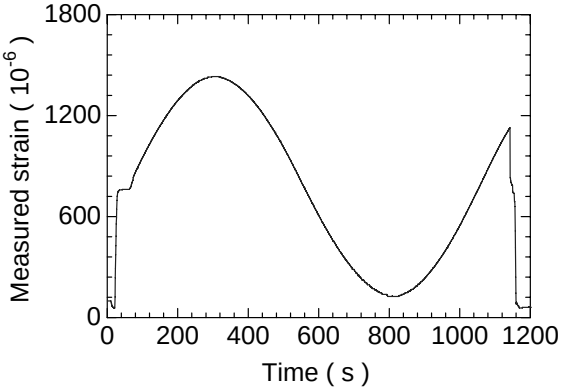

Fig.7 Change in longitudinal strain with time in one cycle for stress amplitude of 50 MPa

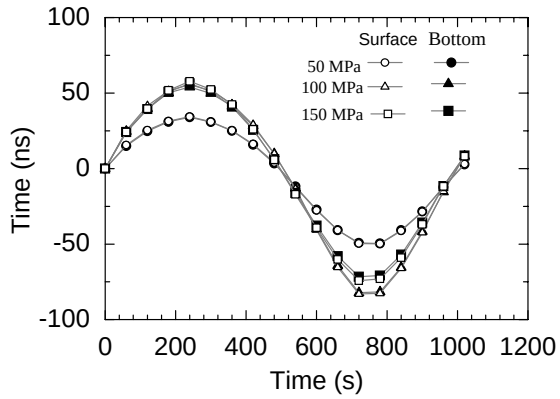

Fig.8 Changes in positions of surface and bottom echoes with time in one cycle for different stresses

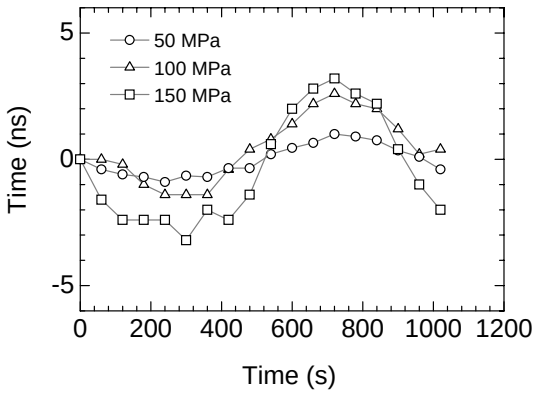

Fig.9 Changes in propagation time of ultrasonic wave from surface to bottom in one cycle for different stresses

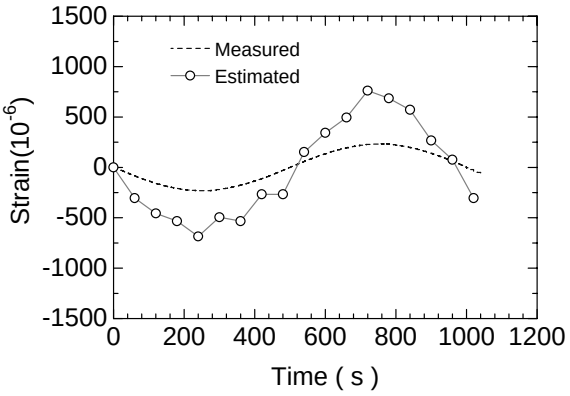

(a) 50 MPa

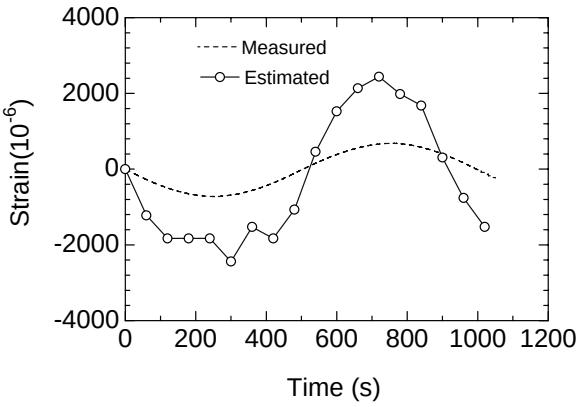

(b) 150 MPa

Fig.10 Measured and estimated transverse strains in one cycle for stress amplitudes of 50 MPa and 150 MPa

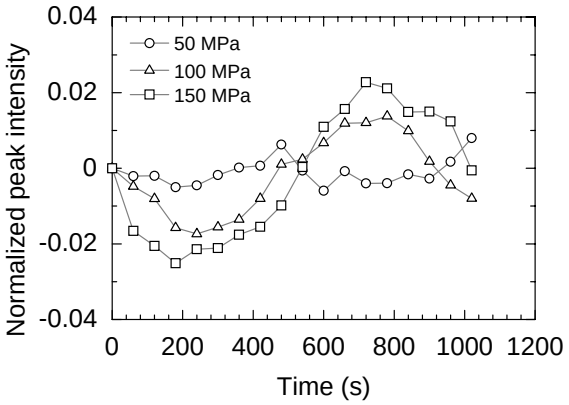

(a) Peak intensity of bottom echo spectrum

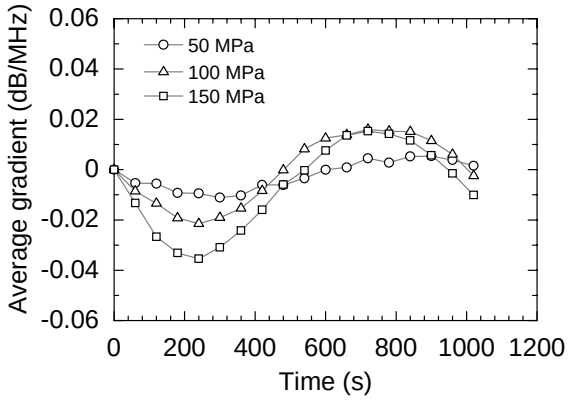

(b) Average gradient of the transfer function

Fig.11 Changes in ultrasonic parameters of bottom echo spectrum with time in one cycle for different stresses

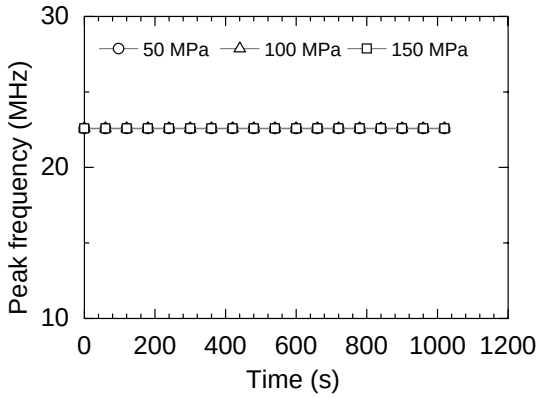

(c) Peak frequency of bottom echo spectrum

Fig.11 (Continued) Changes in ultrasonic parameters of bottom echo spectrum with time in one cycle for different stresses

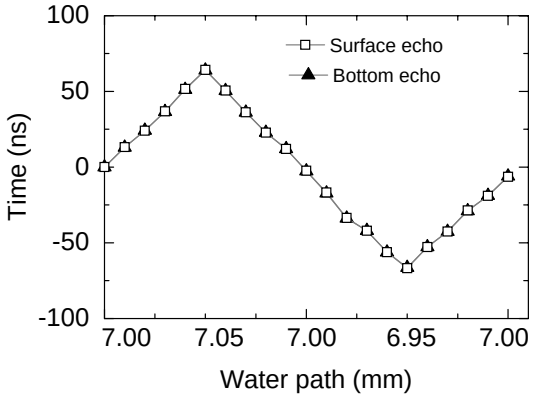

Fig.12 Changes in peak position of surface and bottom echoes from the original water path with the transducer movement

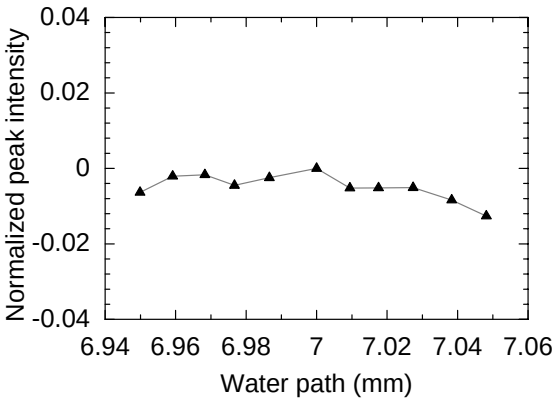

(a) Peak intensity of bottom echo spectrum

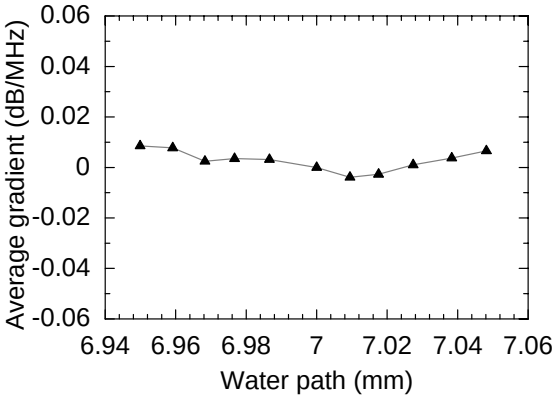

(b) Average gradient of the transfer function

Fig.13 Changes in ultrasonic parameters of bottom echo spectrum with water path without cyclic loading

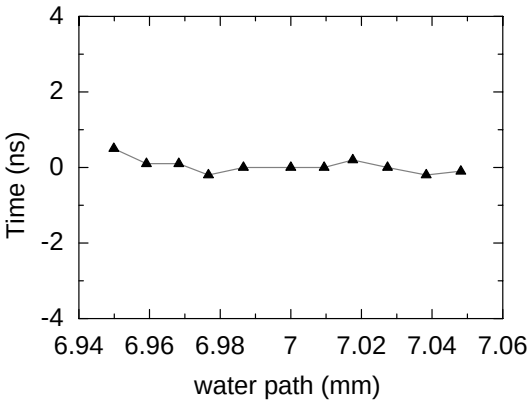

(c) Propagation time of ultrasonic wave

Fig.13 (Continued) Changes in ultrasonic parameters of bottom echo spectrum with water path without cyclic loading

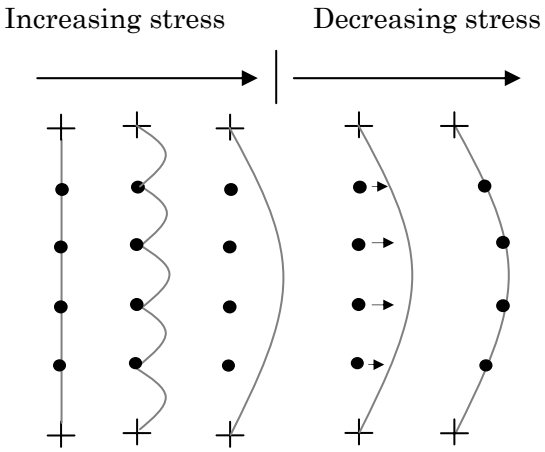

Fig.14 Model of the interaction of dislocations and point defects during the cyclic loading. Solid circles are mobile point defects, crosses are strong pinning points.

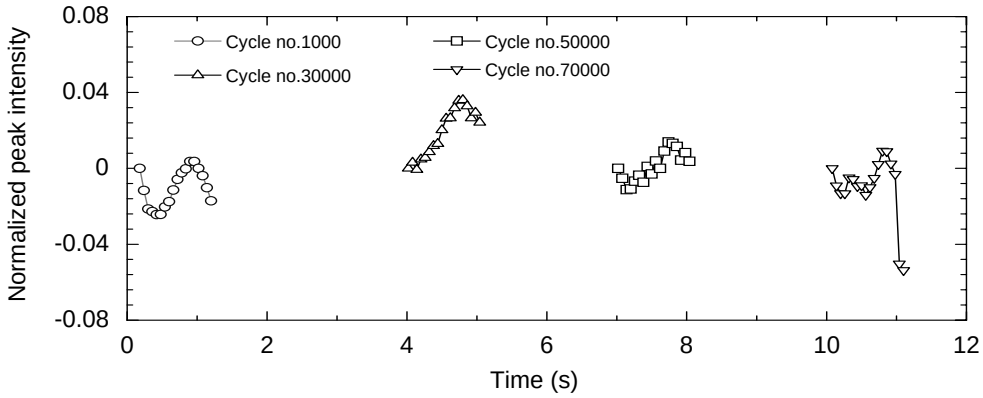

(a) Peak intensity of bottom echo spectrum

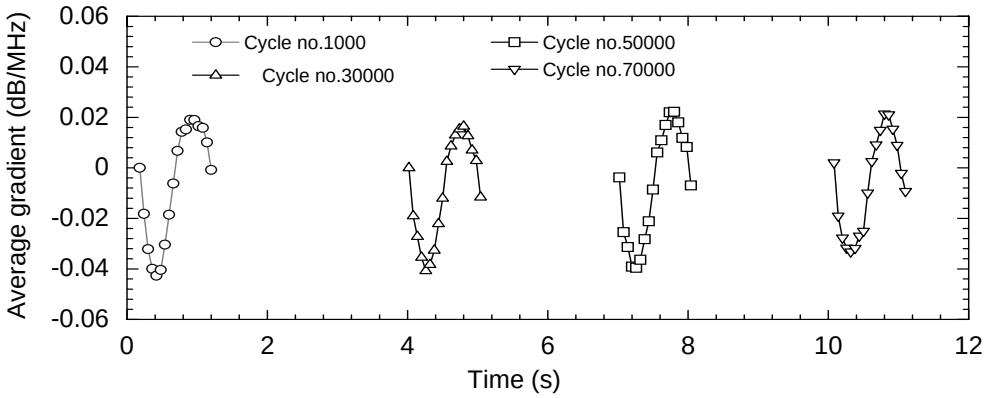

(b) Average gradient of the transfer function

Fig.15 Changes in ultrasonic parameters in one cycle at each stage of fatigue testing for stress amplitude of 150 MPa

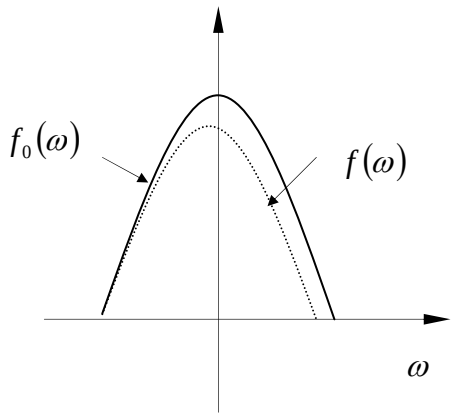

Fig.A-1 Model for change in the Fourier spectrum of the ultrasonic wave